

The Exponential Capacity of Dense Associative Memories

Carlo Lucibello* and Marc Mézard†
Department of Computing Sciences, Bocconi University, Milano, Italy
Bocconi Institute for Data Science and Analytics, Milano, Italy

Recent generalizations of the Hopfield model of associative memories are able to store a number P of random patterns that grows exponentially with the number N of neurons, $P = \exp(\alpha N)$. Besides the huge storage capacity, another interesting feature of these networks is their connection to the attention mechanism which is part of the Transformer architectures widely applied in deep learning. In this work, we consider a generic family of pattern ensembles, and thanks to the statistical mechanics analysis of an auxiliary Random Energy Model, we are able to provide exact asymptotic thresholds for the retrieval of a typical pattern, α_1 , and lower bounds for the maximum of the load α for which all patterns can be retrieved, α_c . Additionally, we characterize the size of the basins of attractions. We discuss in detail the cases of Gaussian and spherical patterns, and show that they display rich and qualitatively different phase diagrams.

I. INTRODUCTION

About forty years ago, John Hopfield introduced a simple model of memory [1] based on N spins interacting by pairs like in a spin glass, but with specifically tailored interactions so that the ground states of the spin-glass are strongly correlated with a set of patterns that one wants to memorize. This allows building an associative memory that retrieves the full information from some partial information. Using statistical physics methods, it was then shown that this model can store up to $\alpha_c N$ independent random patterns in the large N limit, with $\alpha_c \simeq 0.14$ if one uses the simple Hebb rule for defining the interactions [2, 3]. Going beyond pairwise interactions, i.e. introducing p -spin interactions, yields a big increase in the memory capacity which becomes of order N^{p-1} [4–6]. Pushing this strategy further, a family of models with exponential interaction terms leading to exponential capacity has been recently introduced and analyzed in Refs. [7, 8]. While [7] discusses networks with Ising variables, Ref. [8] considers continuous variables and links the dynamics of the system with the attention mechanism one finds in the transformer models [9] now ubiquitous in natural language processing and other domains in machine learning.

Here we perform a statistical mechanics analysis of these modern versions of associative memories. Defining $P = e^{\alpha N}$ the number of patterns, we want to compute the critical value α_c such that, for $\alpha < \alpha_c$ retrieval is possible with high probability in the large N limit. Notice that the precise definition of α_c in presence of an exponentially large number of patterns requires some care, and indeed we will find distinct thresholds depending on whether we request to store all patterns, or we request that a typically chosen pattern can be retrieved.

Following Ramsauer et al. [8], we consider a set of $P = e^{\alpha N}$ patterns $\{\xi^\mu\}_{\mu=1}^P$, $\xi^\mu \in \mathbb{R}^N$, independently and identically distributed according to some distribution $\mathcal{P}(\xi)$, that should be memorized by a network of N neurons. The activities of the neurons are encoded in

a N -dimensional vector \mathbf{x} . Starting from an initial condition $\mathbf{x}_0 \in \mathbb{R}^N$, the recall of a memorized pattern will be based on a gradient descent (GD) procedure in the landscape defined by the energy function

$$E(\mathbf{x}) = -\frac{1}{\lambda} \log \sum_{\mu=1}^P e^{\lambda \mathbf{x} \cdot \xi^\mu} + \frac{1}{2} \|\mathbf{x}\|^2. \quad (1)$$

Notice that with respect to Ref. [8] we exchanged the roles of \mathbf{x} and ξ in order to conform to statistical physics' standard notation.

Considering step size 1 in GD, we obtain the update rule

$$\mathbf{x}_{t+1} = \sum_{\mu} a_t^\mu \xi^\mu, \quad a_t^\mu = \frac{e^{\lambda \mathbf{x}_t \cdot \xi^\mu}}{\sum_{\nu} e^{\lambda \mathbf{x}_t \cdot \xi^\nu}}. \quad (2)$$

Interestingly, this update rule is well known in the recent developments of deep learning [9, 10]. It corresponds to a cross-attention mechanism with a single query $\mathbf{x} = \mathbf{q}$ and identical key and value matrices: $K = V = [\xi^1, \dots, \xi^P]$. In fact, the update rule can be compactly written as $\mathbf{x}_{t+1} = V \text{Softmax}(\mathbf{x}_t^T K)$. The coefficients a_t^μ are commonly called attention scores.

A pattern ξ^μ will be said to be (ϵ) -retrieved if, starting from an initial configuration \mathbf{x}_0 close enough to the pattern, we have $\lim_{t \rightarrow \infty} \frac{1}{N} \|\mathbf{x}_t - \xi^\mu\|^2 < \epsilon$ for some $\epsilon \geq 0$ that we assume to be vanishing for large N . At odds with the standard Hopfield model with $O(N)$ patterns where the retrieved configuration always contains a small fraction of errors compared to the original pattern, here we discuss (asymptotic) perfect retrieval.

At fixed interaction strength λ , we define the single pattern retrieval threshold $\alpha_1(\lambda)$ as the largest value of α for which the probability of retrieving a randomly chosen pattern goes to one in the large N limit. As we argue later, above the threshold the probability goes to zero instead. The other problem we consider is the full retrieval problem, that is determining the maximum number of patterns that the system is able to store. We thus define the capacity threshold $\alpha_c(\lambda)$ as the largest α such

that all $P = e^{\alpha N}$ patterns are retrieved. Clearly we have $\alpha_c \leq \alpha_1$.

In this paper, we derive exact and simple expressions for α_1 , provide bounds on α_c , and study the size of attraction basins, i.e. the maximal distance between \mathbf{x}_0 and the pattern such that retrieval is possible. We shall first explain the general formalism and then apply it to the cases of spherical and Gaussian pattern ensembles.

II. RETRIEVAL OF A TYPICAL PATTERN

We study the capacity in the thermodynamic limit $N \rightarrow \infty$, for patterns that are distributed in such a way that their squared norm is $\|\boldsymbol{\xi}^\mu\|^2 = O(N)$, so that also relevant configurations \mathbf{x} have similar scaling with N . Let us choose one of the patterns at random or deterministically but independently from the sample realization, say $\boldsymbol{\xi}^1$ without loss of generality, and explore the energy landscape in its neighborhood. We are thus interested in the energy $E(\mathbf{x})$ when the overlap of \mathbf{x} with the first pattern, $\mathbf{x} \cdot \boldsymbol{\xi}^1$, is $O(N)$. Its overlaps with each of the $e^{\alpha N} - 1$ other patterns with $\mu \geq 2$ are typically of order \sqrt{N} ; however, as their number is exponentially large, some of these overlaps will also be of order N . It is convenient to separate the two extensive contributions appearing inside the logarithm in the energy function:

$$E(\mathbf{x}) = -\frac{1}{\lambda} \log \left(e^{\lambda \mathbf{x} \cdot \boldsymbol{\xi}^1} + e^{\lambda N \Phi(\mathbf{x})} \right) + \frac{1}{2} \|\mathbf{x}\|^2, \quad (3)$$

where we defined

$$\Phi(\mathbf{x}) = \frac{1}{\lambda N} \log \left(\sum_{\mu=2}^P e^{\lambda \mathbf{x} \cdot \boldsymbol{\xi}^\mu} \right). \quad (4)$$

For given $\boldsymbol{\xi}^1$ and \mathbf{x} independent from the other patterns, the free energy Φ is a random variable whose distribution is induced by the random patterns $\boldsymbol{\xi}^\mu$ with $\mu = 2, \dots, P$. Notice that Φ is minus the free energy density of a Random Energy Model (REM) [11] with $P - 1$ energy levels $E^\mu = \mathbf{x} \cdot \boldsymbol{\xi}^\mu$ and inverse temperature λ . For simplicity, we shall focus hereafter on settings where the distribution of E^μ depends on \mathbf{x} only through its rescaled norm $\rho = \|\mathbf{x}\|/\sqrt{N}$. This is the case for pattern distributions that are rotationally invariant. We note that our approach could be easily extended to the case of factorized pattern distributions. In the thermodynamic limit where $N, P \rightarrow \infty$ with fixed exponential rate α and considering a sequence of \mathbf{x} at fixed rescaled norm ρ , the quantity $\Phi(\mathbf{x})$ converges almost surely to the free-energy density of a REM, $\phi_{\alpha, \rho}(\lambda)$. Standard computations show that it is expressed in terms of the cumulant generating function of the energy levels

$$\zeta_\rho(\lambda) = \lim_{N \rightarrow \infty} \frac{1}{N} \log \mathbb{E}_\xi e^{\lambda \mathbf{x} \cdot \boldsymbol{\xi}} \quad (5)$$

and its Legendre transform

$$\hat{\zeta}_\rho(\varepsilon) = \sup_\lambda [\lambda \varepsilon - \zeta_\rho(\lambda)]. \quad (6)$$

With these definitions, the free-energy density of the REM reads [12]

$$\phi_{\alpha, \rho}(\lambda) = \begin{cases} \frac{\alpha + \zeta_\rho(\lambda)}{\lambda} & \lambda < \lambda_*(\alpha, \rho) \\ \varepsilon_*(\alpha, \rho) & \lambda \geq \lambda_*(\alpha, \rho) \end{cases} \quad (7)$$

where ε_* is the largest ε such that $\hat{\zeta}_\rho(\varepsilon) \leq \alpha$, and $\lambda_* = \hat{\zeta}'_\rho(\varepsilon_*)$. The interpretation of Eq. (7) is that for $\lambda < \lambda_*$ exponentially many patterns contribute to $\phi_{\alpha, \rho}(\lambda)$, while for $\lambda \geq \lambda_*$ it is entirely given by the pattern with the largest overlap $\mathbf{x} \cdot \boldsymbol{\xi}^\mu / N$. This last phase is called condensed phase. For large N we can therefore write

$$E(\mathbf{x}) \approx -\max(\mathbf{x} \cdot \boldsymbol{\xi}^1, N\phi_{\alpha, \rho}(\lambda)) + \frac{1}{2} \|\mathbf{x}\|^2. \quad (8)$$

Whenever $\mathbf{x} \cdot \boldsymbol{\xi}^1$ dominates the max, the energy becomes a quadratic function with minimum in $\boldsymbol{\xi}^1$. Moreover, GD reaches the minimum in one step. The basin of attraction of $\boldsymbol{\xi}^1$ shrinks with increasing α , up to the point where the REM free energy dominates the max even at $\mathbf{x} = \boldsymbol{\xi}^1$ and the pattern is no longer a minimum. We call $r = \|\boldsymbol{\xi}^1\|/\sqrt{N}$, and observe that with high probability r will take the value $r_\xi = \lim_{N \rightarrow \infty} \sqrt{\mathbb{E} \|\boldsymbol{\xi}\|^2 / N}$. We thus have a simple criterium to identify the critical value α_1 such that for $\alpha < \alpha_1$ retrieval of $\boldsymbol{\xi}^1$ is possible:

$$\alpha_1(\lambda) = \sup \{ \alpha : r_\xi^2 > \phi_{\alpha, r_\xi}(\lambda) \}. \quad (9)$$

Remarkably, we could derive this exact threshold thanks to a simple inspection of the energy function, bypassing calculations involving the dynamical rule or even quenched free energy computations à la Ref. [13]. In fact, due to the exponential terms, the signal-vs-noise balance becomes an all-or-nothing one. On the other hand, let us mention a subtlety of our derivation: in the discussion regarding $\Phi(\mathbf{x})$, we assumed the choice of \mathbf{x} to be independent from $\boldsymbol{\xi}^{2:P}$. Therefore one cannot be sure that Eq. (8) holds for all \mathbf{x} in a neighborhood of $\boldsymbol{\xi}^1$. However it does hold for $\mathbf{x} = \boldsymbol{\xi}^1$. The continuity of the involved quantities then implies that for $\alpha < \alpha_1(\lambda)$ we have convergence to the pattern for all initial configurations within a non-vanishing (and extensive) ball centered at $\boldsymbol{\xi}^1$. What happens when the pattern is not retrieved instead? Ramsauer et al. [8] show that in this case the attention scores become approximately flat and the dynamics converges to the barycenter of the patterns that is approximately the origin in our case.

III. RETRIEVAL OF ALL PATTERNS

We now consider the stronger requirement that *all patterns* can be successfully retrieved. While in the standard Hopfield model and its polynomial generalizations,

single and all-patterns retrieval thresholds coincide since all patterns can be considered typical, in presence of an exponential number of patterns one needs to control exponentially rare events.

In order to derive a lower bound, $\alpha_c^{\text{lb}} \leq \alpha_c$, for the critical value of α such that all patterns are retrieved, we use a union bound: if p_1 is the probability of retrieval of one pattern, the probability p_c that all patterns are retrieved verifies $1 - p_c \leq e^{\alpha N} (1 - p_1)$. As we have seen, $1 - p_1$ is the probability that the free-energy of the REM with $P - 1$ energy levels $E^\mu = \xi^1 \cdot \xi^\mu$ (with $\mu \neq 1$) is larger than $\|\xi^1\|^2$. In order to control p_c , we thus need to compose the large deviations for the norm of the reference pattern with the large deviations for the REM free-energy.

As proven in Ref. [12] (see also [14]), if $\|\xi^1\| = r\sqrt{N}$ and $\zeta_r(\lambda)$ is defined for all $\lambda \in \mathbb{R}$, differentiable, and strictly convex, then the distribution of the REM free-energy density ϕ satisfies a large deviation principle given by $P(\phi) = e^{-N I_{\alpha,r,\lambda}(\phi)}$ with

$$I_{\alpha,r,\lambda}(\phi) = \begin{cases} +\infty & \phi < \phi_{\alpha,r}(\lambda) \\ 0 & \phi = \phi_{\alpha,r}(\lambda) \\ \zeta_r(\phi) - \alpha & \phi > \phi_{\alpha,r}(\lambda). \end{cases} \quad (10)$$

Let us call $\tilde{I}(r)$ the large deviation function for $\|\xi^1\|/\sqrt{N}$. Accounting for the fluctuations of r and for the fluctuations of the REM free energy conditioned on the value of r , it is easy to show that $1 - p_1 = e^{-NA(\alpha,\lambda)}$ for large N . The rate function $A(\alpha, \lambda)$ is given by

$$A(\alpha, \lambda) = \inf_{r \in [0, \infty)} \left[\tilde{I}(r) + \inf_{\phi: \phi > r^2} I_{\alpha,r,\lambda}(\phi) \right]. \quad (11)$$

Therefore, the union bound provides a lower bound for the all-patterns storage capacity in the form

$$\alpha_c^{\text{lb}} = \sup\{\alpha : A(\alpha, \lambda) - \alpha > 0\} \quad (12)$$

We note that since $\alpha_c^{\text{lb}} \leq \alpha_c \leq \alpha_1$, when $\alpha_c^{\text{lb}} = \alpha_1$ the bound turns into an equality. As we will show, this is always the case for spherical patterns, while for Gaussian patterns there is a gap at any λ .

IV. BASINS OF ATTRACTION

The full analytic computation of attraction basins requires following a trajectory in time. This is a complicated task, which has not been done in the standard Hopfield model, and which is beyond the reach of our method. However, we can obtain a good indication of the size of attraction basins using the energy decomposition of Eq. (3). Consider an initialization \mathbf{x} sampled uniformly at random conditioned on a given norm and with given angle from the first pattern: $\|\mathbf{x}\| = \rho\sqrt{N}$, $\cos(\theta) = \mathbf{x} \cdot \xi^1 / \|\mathbf{x}\| \|\xi^1\|$. Eq. (3)

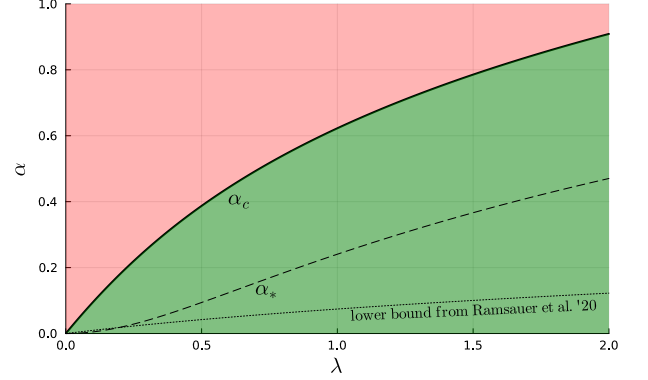


FIG. 1. Phase diagram for spherical patterns. All the patterns are retrieved in the green region $\alpha < \alpha_c = \alpha_c^{\text{lb}} = \alpha_1$. We also show the line $\alpha_*(\lambda)$ where the REM condensation occurs, and the lower bound for the capacity from Ref. [8].

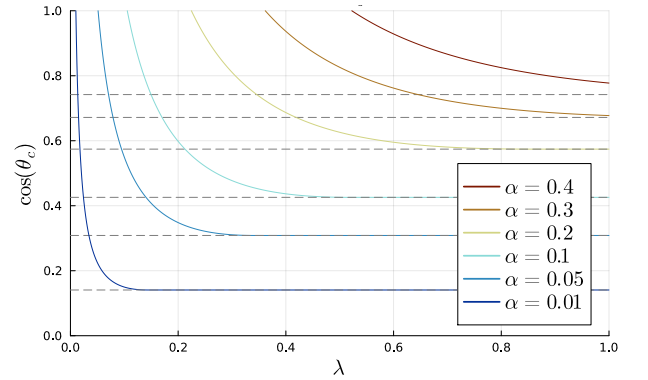


FIG. 2. Maximum angle $\theta_c(\alpha, \lambda)$ between a typical pattern and a random initialization such that the pattern is retrieved with high probability. The patterns here follow a spherical distribution and the configuration is also initialized on the hypersphere. Horizontal lines correspond to the angle of the nearest pattern.

implies that if $\rho r_\xi \cos(\theta) > \phi_{\alpha,\rho}(\lambda)$ then the first pattern dominates, and the gradient is $\mathbf{x} - \xi^1$. If the pattern is stable, i.e. $r_\xi^2 > \phi_{\alpha,r_\xi}(\lambda)$, it is retrieved after one step of GD with step size 1. On the other hand, if $\rho r_\xi \cos(\theta) > \phi_{\alpha,\rho}(\lambda)$, the energy is dominated by the all other patterns. Then one needs to study the multi-step dynamics in order to see the final point of GD. Therefore, at large N , the condition $\rho r_\xi \cos(\theta) = \phi_{\alpha,\rho}(\lambda)$ identifies the transition line in the $\rho - \theta$ plane separating a region where with high probability the pattern is retrieved in one step when starting from random initial condition, and a region where we conjecture that the pattern is not retrieved. We call θ_c the critical angle value, omitting the dependence on all other parameters. We remark that this argument does not apply to all starting points with given ρ and θ : a more fine-grained analysis of the attraction basin requires controlling the rare events.

It is interesting to relate $\cos \theta_c$ to the distance of the

nearest pattern. Due to the condensation transition we have $\lim_{\lambda \rightarrow \infty} \phi_{\alpha, \rho}(\lambda) = \varepsilon_*(\alpha, \rho) = \rho c_{max}(\alpha)$ where $c_{max}(\alpha)$ is the maximum (in the thermodynamic limit) of the overlaps $\{\mathbf{x} \cdot \boldsymbol{\xi}^\mu / N\}_{\mu=2}^{e^{\alpha N}}$, now assuming $\|\mathbf{x}\| = \sqrt{N}$. The value $c_{max}(\alpha)$ is the generalization of the Gilbert-Varshamov distance, well-known in error correcting codes. Using standard methods [15], one can show that this limit is the largest root of $S_\alpha^{ann}(c) = 0$, where $S_\alpha^{ann}(c) = \alpha - \hat{\zeta}_1(c)$ (see SM B). For given ρ , the basin size θ_c increases monotonically with λ up to its ρ -independent maximum size $\cos(\theta_c) = c_{max}(\alpha)$ (assuming $r_\xi = 1$).

V. APPLICATIONS TO PATTERN ENSEMBLES

A. Spherical patterns

For spherical patterns, i.e. with uniform distribution on the sphere $\|\boldsymbol{\xi}\|^2 = N$, the cumulant generating function and its Legendre transform are computed in SM C. The threshold $\alpha_1(\lambda)$ for the retrieval of a typical pattern given by Eq. (9) is identified by $\phi_{\alpha_1, 1}(\lambda) = 1$. It turns out that, in this case, the large deviation function of the REM free-energy is infinite, except for the point $\phi = \phi_{\alpha, r}(\lambda)$ where it vanishes. Therefore there is a unique retrieval transition line, $\alpha_1 = \alpha_c$. See SM C for the details.

Fig. 1 shows the phase diagram in the $\alpha - \lambda$ plane. One should notice that there is no upper limit to the capacity: at large λ , one finds $\alpha_c \sim 0.5 \log \lambda$. Of course, as we shall see later, in the high- λ high- α regime the basins of attraction become very small. Besides the $\alpha_c = \alpha_1$ line, we also report the weaker (but rigorous) lower bound to α_c obtained by extrapolating Ref. [8] results to large N (see SM E). Notice that $\alpha_* < \alpha_c$, therefore the destabilization of a pattern is always due to the contribution of exponentially many other patterns. The numerical experiments in SM F corroborate the theoretical findings.

In Fig. 2 we show the critical size for the basins discussed previously. Considering a typical pattern, recovery is possible from a random initial condition on the sphere at an angle θ , as long as $\theta < \theta_c(\alpha, \lambda)$. The expression for θ_c is given in SM C. We see that the basin size decreases monotonically with α as expected. For a given α and increasing λ , we find 3 regimes: 1) No retrieval for $\lambda < \lambda_c(\alpha)$; 2) Monotonically increasing basin size for $\lambda_c(\alpha) < \lambda < \lambda_*(\alpha)$; 3) Basin size frozen to $\theta_*(\alpha)$ for $\lambda > \lambda_*(\alpha)$. The value $\theta_*(\alpha)$ corresponds to the typical distance of nearest patterns. The REM is in a condensed phase in this last regime.

Gaussian patterns

In the case of Gaussian patterns, even if the typical norm of a pattern is the same as for spherical patterns,

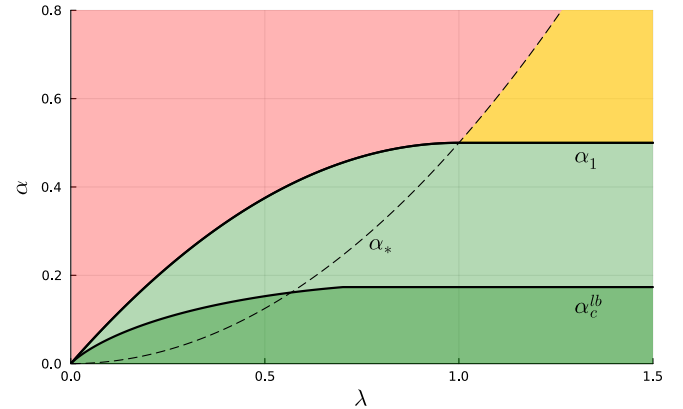


FIG. 3. Phase diagram for Gaussian patterns. We show the retrieval threshold of a typical pattern, α_1 , the lower bound α_c^{lb} to the all patterns retrieval capacity, and the REM condensation line α_* .

this norm can fluctuate and this leads to larger deviations from the typical behavior. The phase diagram derived in SM D and summarized in Fig. 3 thus differs significantly from the one for spherical patterns. The capacity of retrieval for typical patterns, α_1 , saturates at $\lambda = 1$ to the value $\alpha_1 = 1/2$. The lower bound to α_c no longer coincides with α_1 . It saturates at large λ to the value $\alpha_c^{lb}(\lambda = \infty) = \log 2 / 4$. Finally, in the phase $\alpha > \alpha_1$ where the patterns are not retrieved, the dominating REM term in the energy can be either in a condensed phase (known as “static 1RSB” phase in spin glass theory, yellow in the plot) or not (“dynamic 1RSB” phase, red) depending on the value of λ .

VI. SCALED DOT-PRODUCT

The dot-product found in the softmax operation of Transformer architectures is commonly scaled by a \sqrt{N} factor [9] so that totally uncorrelated keys and queries give an $O(1)$ exponent. Therefore we consider a scaling regime where $\lambda = \tilde{\lambda}/N^a$ for some $a \in (0, 1)$. The energy function now reads

$$E(\mathbf{x}) = -\frac{N^a}{\tilde{\lambda}} \log \sum_\mu e^{\frac{\tilde{\lambda}}{N^a} \mathbf{x} \cdot \boldsymbol{\xi}^\mu} + \frac{1}{2} \|\mathbf{x}\|^2. \quad (13)$$

The interesting regime is now when the number of patterns scales as $P = \exp(\tilde{\alpha} N^{1-a})$ so that we have a competition between the REM contribution Φ and the signal term $\frac{\tilde{\lambda}}{N^a} \|\boldsymbol{\xi}^1\|^2$ in Eq. (3) when $\mathbf{x} = \boldsymbol{\xi}^1$. With this assumption, in fact, we have $\lambda N \Phi = N^{1-a} \tilde{\alpha}$ for any pattern ensemble. In the auxiliary REM, the number of patterns is too small for observing significant large deviations in the energy levels, therefore its free energy is trivially given by its entropy. The typical pattern retrieval threshold in this setting always coincides with the

all-patterns retrieval one, and they take the simple value $\tilde{\alpha}_1 = \tilde{\alpha}_c = \tilde{\lambda}$. In SM F we present numerical experiments supporting this result.

VII. CONCLUSIONS

Dense associative memories have exponential capacity, at the cost of using an energy function that takes an exponential number of operations. This gives a completely new regime where we can use statistical physics to analyze the energy landscape, and determine the asymptotic memory capacity of large networks, as well as their attraction basins for zero-temperature dynamics starting from random configurations. Generalizing these results to properties of the free-energy landscape (at finite temperature), or to the worst-case initial conditions is an interesting challenge: subtle effects due to the exponential number of patterns, and resulting rare events, are to be taken into account. On the other hand it should be possible to establish rigorously our zero-temperature results, and to extend them to factorized pattern distributions, such as the case of binary neurons $\{-1, +1\}^N$. Finally, it would be interesting to extend the study to patterns generated from a hidden-manifold [16], and to explore implications for Transformer architectures.

2015, *San Diego, CA, USA, May 7-9, 2015, Conference Track Proceedings*, edited by Y. Bengio and Y. LeCun (2015).

- [11] B. Derrida, *Physical Review B* **24**, 2613 (1981).
- [12] M. Fedrigo, F. Flandoli, and F. Morandin, *Annali di Matematica Pura ed Applicata* **186**, 381 (2007).
- [13] D. J. Amit, H. Gutfreund, and H. Sompolinsky, *Annals of Physics* **173**, 30 (1987).
- [14] E. Gardner and B. Derrida, *Journal of Physics A: Mathematical and General* **22**, 1975 (1989).
- [15] M. Mézard and A. Montanari, *Information, physics, and computation* (Oxford Univ. Press, 2009).
- [16] M. Negri, C. Lauditi, G. Perugini, C. Lucibello, and E. Malatesta, (2023), arXiv:2303.16880 [cond-mat.dis-nn].
- [17] M. Mézard, G. Parisi, and M. A. Virasoro, *Spin glass theory and beyond: An Introduction to the Replica Method and Its Applications*, Vol. 9 (World Scientific Publishing Company, 1987).
- [18] M. Pastore, *Replicas in complex systems: applications to large deviations and neural networks*, Ph.D. thesis (2021).

* carlo.lucibello@unibocconi.it

† marc.mezard@unibocconi.it

- [1] J. J. Hopfield, *Proceedings of the National Academy of Sciences* **79**, 2554 (1982), publisher: *Proceedings of the National Academy of Sciences*.
- [2] D. J. Amit, H. Gutfreund, and H. Sompolinsky, *Physical Review A* **32**, 1007 (1985).
- [3] D. J. Amit, H. Gutfreund, and H. Sompolinsky, *Physical Review Letters* **55**, 1530 (1985).
- [4] E. Gardner, *Journal of Physics A: Mathematical and General* **20**, 3453 (1987).
- [5] D. Krotov and J. J. Hopfield, *Advances in Neural Information Processing Systems*, 1180 (2016).
- [6] E. Agliari, L. Albanese, F. Alemanno, A. Alessandrelli, A. Barra, F. Giannotti, D. Lotito, and D. Pedreschi, arXiv preprint arXiv:2211.14067 (2022).
- [7] M. Demircigil, J. Heusel, M. Löwe, S. Uppgang, and F. Vermet, *Journal of Statistical Physics* **168**, 288 (2017), arXiv: 1702.01929.
- [8] H. Ramsauer, B. Schäfl, J. Lehner, P. Seidl, M. Widrich, L. Gruber, M. Holzleitner, T. Adler, D. Kreil, M. K. Kopp, G. Klambauer, J. Brandstetter, and S. Hochreiter, in *International Conference on Learning Representations* (2021).
- [9] A. Vaswani, N. Shazeer, N. Parmar, J. Uszkoreit, L. Jones, A. N. Gomez, L. Kaiser, and I. Polosukhin, in *Advances in neural information processing systems* (2017) pp. 5998–6008.
- [10] D. Bahdanau, K. Cho, and Y. Bengio, in *3rd International Conference on Learning Representations, ICLR*

Supplemental Information

CONTENTS

| | |
|--|----|
| I. Introduction | 1 |
| II. Retrieval of a typical pattern | 2 |
| III. Retrieval of all patterns | 2 |
| IV. Basins of attraction | 3 |
| V. Applications to pattern ensembles | 4 |
| A. Spherical patterns | 4 |
| Gaussian patterns | 4 |
| VI. Scaled dot-product | 4 |
| VII. Conclusions | 5 |
| References | 5 |
| A. Analysis of the REM | 6 |
| B. Typical distances | 8 |
| C. Spherical patterns | 9 |
| 1. Typical case | 9 |
| 2. All patterns retrieval | 10 |
| 3. Attraction basins | 11 |
| D. Gaussian patterns | 11 |
| 1. Typical case | 11 |
| 2. All patterns retrieval | 13 |
| 3. Attraction basins and typical distances | 14 |
| E. Storage capacity lower bound from Ramsauer et al. '20 | 15 |
| F. Numerical Experiments | 17 |
| 1. Typical pattern retrieval | 17 |
| 2. Basins | 17 |
| 3. Scaled dot-product | 18 |

Appendix A: Analysis of the REM

We briefly recall the standard analysis of the REM (see [11, 15]) with the present notations. We consider $P = \exp(\alpha N)$ energy levels E^μ that are independently and identically drawn from a distribution induced by the scalar products $\xi^\mu \cdot \mathbf{x}$. This distribution can be characterized by a rate function $\hat{\zeta}_\rho(\varepsilon)$ for large N , which means that the probability density to find an energy level E^μ in the interval $[N\varepsilon, N\varepsilon + d\varepsilon]$ is given by $C e^{-N\hat{\zeta}_\rho(\varepsilon)}$, where $\hat{\zeta}_\rho(\varepsilon)$ is a non-negative function equal to zero at one point ε_0^ρ , the typical energy density of a random pattern. C is a constant that is irrelevant for our computation, as $(1/N) \log C \rightarrow 0$ in the large N limit. ρ is a parameter characterizing the distribution of the energy levels and is given by the scaled norm of the configuration we are considering, $\rho = \|\mathbf{x}\|/\sqrt{N}$.

We introduce a parameter λ that plays the role of an inverse temperature and we want to compute the asymptotic average free-energy density

$$\phi_{\alpha,\rho}(\lambda) = \lim_{N \rightarrow +\infty} \frac{1}{\lambda N} \mathbb{E} \log \left(\sum_{\mu=2}^P e^{\lambda E^\mu} \right). \quad (\text{A1})$$

Notice that at odds with the usual convention, the energy here doesn't take a minus sign in the exponent. A relevant quantity related to the free energy is the density of energy levels for a given realization, $\mathcal{N}(\varepsilon)$, and its expectation

$$\mathbb{E} \mathcal{N}(\varepsilon) \approx e^{N(\alpha - \hat{\zeta}_\rho(\varepsilon))}, \quad (\text{A2})$$

where \approx denotes equality up to subleading terms for large N . In fact, from this one deduces the annealed average of the partition function

$$\mathbb{E} Z = \int d\varepsilon \mathbb{E} [\mathcal{N}(\varepsilon)] e^{\lambda N \varepsilon} \approx e^{N(\alpha + \zeta_\rho(\lambda))}, \quad (\text{A3})$$

with $\zeta_\rho(\lambda)$ the Legendre transform of $\hat{\zeta}_\rho(\varepsilon)$:

$$\zeta_\rho(\lambda) = \sup_{\varepsilon} \left[\lambda \varepsilon - \hat{\zeta}_\rho(\varepsilon) \right]. \quad (\text{A4})$$

Using the fact that the energies are independent random variables and the second moment method, one can show [11] that $\frac{1}{N} \log \mathcal{N}(\varepsilon) \rightarrow \alpha - \hat{\zeta}(\varepsilon)$ almost surely whenever $\alpha - \hat{\zeta}(\varepsilon) > 0$, and gives $-\infty$ otherwise. This amounts to saying that the count of the energy levels in a typical sample can be obtained (at the exponential order) from the annealed average when the latter is larger than one, and it is zero otherwise. From this observation, one can deduce the expression for the quenched free energy density $\phi_{\alpha,\rho}(\lambda) = \lim_{N \rightarrow \infty} \mathbb{E} \log Z / (N \lambda)$ written in Eq. (7) of the Main Text. Notice that, when $\lambda < \lambda_*$, there is an exponential number of levels μ that contribute to the partition function and the entropy density is strictly positive. On the contrary, when $\lambda > \lambda_*$ there occurs a condensation phenomenon: only the levels with energy density $\varepsilon_* = \sup\{\varepsilon : \alpha - \hat{\zeta}(\varepsilon) > 0\}$ contribute to the free energy, and the entropy density vanishes. We now show how to obtain the same result for the free energy using the replica method, generalizing the derivation in Refs. [11, 15]. It is convenient to use rotational invariance and rewrite the free energy as

$$\phi_{\alpha,\rho}(\lambda) = \lim_{N \rightarrow \infty} \frac{1}{\lambda N} \mathbb{E} \log \sum_{\mu} e^{\lambda \rho \sqrt{N} \xi_1^\mu}. \quad (\text{A5})$$

It is clear that the ρ dependence could be reabsorbed in λ one (or vice-versa), but we will keep both parameters for consistency with the main discussion. We then consider an integer number $n > 0$ of replicas, with n to be sent to zero by analytical continuation at the end of the computation. The average replicated partition function reads

$$\mathbb{E} Z^n = \mathbb{E} \sum_{\mu_1, \dots, \mu_n} e^{\lambda \rho \sqrt{N} \sum_{a=1}^n \xi_1^{\mu_a}}. \quad (\text{A6})$$

In order to decouple the average over patterns, we introduce the variables m_μ defined by $m_\mu = \sum_a \delta_{\mu_a, \mu}$ for a given choice of the labels μ_a . Defining the combinatorial factor

$$M(\{m_\mu\}_\mu) = \sum_{\{\mu_a\}_a} \prod_{\mu} \delta(m_\mu - \sum_a \delta_{\mu_a, \mu}), \quad (\text{A7})$$

we obtain

$$\mathbb{E} Z^n = \mathbb{E} \sum_{\{n_\mu\}_\mu} M(\{m_\mu\}_\mu) e^{\sum_\mu m_\mu \rho \sqrt{N} \xi_1^\mu} \quad (\text{A8})$$

$$= \sum_{\{m_\mu\}_\mu} M(\{m_\mu\}_\mu) e^{N \sum_\mu \zeta_\rho(\lambda m_\mu)}, \quad (\text{A9})$$

where $\zeta_\rho(\lambda)$ is the generating function given by the single pattern expectation

$$\zeta_\rho(\lambda) = \lim_{N \rightarrow \infty} \frac{1}{N} \log \mathbb{E}_{\xi} e^{\sqrt{N} \lambda \rho \xi_1}. \quad (\text{A10})$$

Notice that this is the same $\zeta_\rho(\lambda)$ introduced in Eq. (A4) as a Legendre transform. We will now make an ansatz corresponding to one step of replica symmetry breaking (1RSB) [15, 17] for the values of m_μ dominating the summation.

1RSB ansatz: *The n replicas μ_a are divided into n/m groups of size m . Within a group, all μ_a are the same. Different groups have different μ_a . Therefore $m_\mu = m$ for $\frac{n}{m}$ of the patterns, and $m_\mu = 0$ for the others.*

The parameter m , which has to be optimized, is called the Parisi 1RSB parameter. With this ansatz we have $M = e^{n\frac{\alpha}{m}N}$, from which one obtains

$$\phi_{\alpha,\rho}(\lambda) = \frac{1}{\lambda} \inf_{m \in [0,1]} \left[\frac{\alpha}{m} + \frac{1}{m} \zeta_\rho(\lambda m) \right]. \quad (\text{A11})$$

For any given ρ , the optimal value for the Parisi parameter is increasing in α . Moreover, we also assume the monotonicity of ζ_ρ , which implies that the optimal m is monotonous in λ as well. We now define as $m_*(\alpha, \rho, \lambda)$ the value of m obtained imposing a stationarity condition in Eq. (A11):

$$-\frac{\alpha}{m_*^2} - \frac{1}{m_*^2} \zeta_\rho(\lambda m_*) + \frac{\lambda}{m_*} \zeta'_\rho(\lambda m_*) = 0 \quad (\text{A12})$$

The condensation threshold $\lambda_*(\alpha, \rho)$ is defined by the value of λ for which the stationary m is exactly one:

$$m_*(\alpha, \rho, \lambda_*) = 1. \quad (\text{A13})$$

Solving the same equation for α instead yields the equivalent parametrization of the critical surface $\alpha_*(\rho, \lambda)$. The optimal value of m constrained to the interval $[0, 1]$ in Eq. (A11) is then given by

$$m(\alpha, \rho, \lambda) = \begin{cases} 1 & \lambda < \lambda_*(\alpha, \rho) \\ m_*(\alpha, \rho, \lambda) & \lambda \geq \lambda_*(\alpha, \rho). \end{cases} \quad (\text{A14})$$

The two phases at $\lambda < \lambda_*$ and $\lambda > \lambda_*$ are called dynamical and static 1RSB phase respectively. The final result is given by Eq. (A11), to be evaluated at the optimal value of m given in Eq. (A14).

The equivalence between the free energy expression in Eq. (A11) and the one given in Eq. (7) of the Main Text is not immediately obvious for $\lambda < \lambda_*$ and it is due to the general Legendre structure of the 1RSB formalism. Considering the free energy functional as function of m , in our case $\phi(m) = \frac{1}{\lambda} (\frac{\alpha}{m} + \frac{1}{m} \zeta_\rho(\lambda m))$, one can in fact show [15] that it can be decomposed in a complexity and energy contribution, $\phi(m) = \frac{1}{\lambda m} (\Sigma(\varepsilon(m)) + \lambda m \varepsilon(m))$. Since $\frac{\partial \phi}{\partial \varepsilon} = 0$ due to the stationarity of the action, we have $\frac{\partial \phi}{\partial m} = -\frac{1}{\lambda m^2} \Sigma(\varepsilon(m))$. Therefore, Eq. (A12) selects the value m_* which gives zero complexity and the maximum allowed energy value ε_* . This completes the replica description of the average free energy of the REM.

The replica analysis can be extended to the computation of the large deviation function. This is done considering the partition function at finite n , and using a 1RSB ansatz to obtain

$$G_{\alpha,\rho,\lambda}(n) = \lim_{N \rightarrow \infty} \frac{1}{N} \log \mathbb{E} Z^n. \quad (\text{A15})$$

Thanks to the Gärtner-Ellis theorem, one can then perform a Legendre transform and obtain the convex-hull $\hat{G}_{\alpha,\rho,\lambda}(\phi)$ of the true rate function $I_{\alpha,\rho,\lambda}(\phi)$. Unfortunately, in the uncondensed phase $\lambda < \lambda_*$, the convex-hull \hat{G} differs from the expression for $I_{\alpha,\rho,\lambda}$ proved by in Ref. [12] and reported in Eq. (10) of the Main Text. For a thorough analysis of the large deviations in the REM as computed by the replica method, we refer the reader to Chap. 2 in Ref. [18].

Appendix B: Typical distances

The typical distance between a configuration and the nearest patterns is related to the attraction basin size at large λ and can be studied as follows. We take a configuration \mathbf{x} with $\|\mathbf{x}\| = \sqrt{N}$ as the reference configuration, since,

as argued in Section of the Main Text discussing basins of attraction, it is sufficient to consider the case $\rho = 1$. We could also take $\mathbf{x} = \boldsymbol{\xi}^1$, the only requirement is that \mathbf{x} is chosen independently from the $\mu \geq 2$ patterns. We study the overlaps $c^\mu = \mathbf{x} \cdot \boldsymbol{\xi}^\mu / N$. Conditioning on \mathbf{x} , the c^μ are independent random variables. For a given realization of the patterns, let us call $N(c)$ the number of patterns with overlap $c^\mu = c$. We first compute the annealed average

$$\mathbb{E}_{\boldsymbol{\xi}^{2:P}} N(c) = \mathbb{E}_{\boldsymbol{\xi}^{2:P}} \sum_{\mu \geq 2} \delta(Nc - \mathbf{x} \cdot \boldsymbol{\xi}^\mu) \quad (B1)$$

$$= \mathbb{E}_{\boldsymbol{\xi}^{2:P}} \sum_{\mu=2}^P \int \frac{dv}{2\pi/N} e^{-Nvc + v \boldsymbol{\xi}^1 \cdot \boldsymbol{\xi}^\mu} \quad (B2)$$

$$= \int \frac{dv}{2\pi/N} e^{N(\alpha - vc + \zeta_1(v))} \quad (B3)$$

where the integral over v is along the imaginary axis. Using the saddle point method we obtain

$$S_\alpha^{ann}(c) = \lim_{N \rightarrow \infty} \frac{1}{N} \log \mathbb{E}_{\boldsymbol{\xi}^{2:P}} N(c) = \text{st}_v [\alpha - vc + \zeta_1(v)] = \alpha - \hat{\zeta}_1(c), \quad (B4)$$

where st denotes the stationary point (a minimum in this case). Because of the independence of the random variables c^μ , the usual REM argument shows that the random variable $\frac{1}{N} \log N(c)$ converges almost surely to a deterministic quantity:

$$S_\alpha(c) = \lim_{N \rightarrow \infty} \frac{1}{N} \log N(c) = \begin{cases} S_\alpha^{ann}(c) & S_\alpha^{ann}(c) \geq 0 \\ -\infty & S_\alpha^{ann}(c) < 0 \end{cases} \quad (B5)$$

Therefore $c_{max}(\alpha)$ is obtained as the largest root of $S_\alpha(c_{max}) = 0$. Notice that this is exactly the condition $\alpha = \hat{\zeta}_1(\varepsilon_*)$ determining $\varepsilon_*(\alpha, \rho = 1)$. In fact, the largest physical (non-negative complexity) energy level corresponds to the maximum overlap $c_{max}(\alpha) = \varepsilon_*(\alpha, \rho = 1)$.

Appendix C: Spherical patterns

1. Typical case

Consider the case where patterns $\boldsymbol{\xi}^\mu \in \mathbb{R}^N$ are uniformly distributed on the sphere $\|\boldsymbol{\xi}^\mu\|^2 = N$, and choose a vector \mathbf{x} such that $\|\mathbf{x}^2\| = N\rho^2$. Using rotational invariance, the distribution of the energy levels $E^\mu(\mathbf{x}) = \mathbf{x} \cdot \boldsymbol{\xi}^\mu$ depends on \mathbf{x} only through ρ . One can choose the axes so that $E^\mu(\mathbf{x}) = \rho\sqrt{N}\xi_1^\mu$. The probability density of this energy is expressed by the large deviation function

$$\hat{\zeta}_\rho(\varepsilon) = - \lim_{N \rightarrow \infty} \frac{1}{N} \log \int \prod_i d\xi_i \delta\left(N - \sum_i \xi_i^2\right) \delta\left(\varepsilon - \frac{\rho\xi_1}{\sqrt{N}}\right). \quad (C1)$$

It is easier to compute its Legendre transform

$$\zeta_\rho(\lambda) = \lim_{N \rightarrow \infty} \frac{1}{N} \log \int \prod_i d\xi_i \delta\left(N - \sum_i \xi_i^2\right) e^{\lambda\rho\xi_1\sqrt{N}}. \quad (C2)$$

Standard field theoretical calculations and saddle point evaluation lead to

$$\zeta_\rho(\lambda) = \frac{1}{2} \left(\sqrt{1 + 4\lambda^2\rho^2} - 1 - \log \left[\frac{1 + \sqrt{1 + 4\lambda^2\rho^2}}{2} \right] \right). \quad (C3)$$

Performing the inverse Legendre transform one gets

$$\hat{\zeta}_\rho(\varepsilon) = -\frac{1}{2} \log \left(1 - \frac{\varepsilon^2}{\rho^2} \right). \quad (C4)$$

According to Eq. (7) of the Main Text, the REM free-energy density is given by

$$\phi_{\alpha,\rho}(\lambda) = \begin{cases} \frac{\alpha}{\lambda} + \frac{1}{2\lambda} \left(\sqrt{1+4\lambda^2\rho^2} - 1 - \log \left[\frac{1+\sqrt{1+4\lambda^2\rho^2}}{2} \right] \right) & \lambda < \lambda_*(\alpha, \rho) \\ \rho \sqrt{1-e^{-2\alpha}} & \lambda \geq \lambda_*(\alpha, \rho), \end{cases} \quad (\text{C5})$$

where

$$\lambda_*(\alpha, \rho) = \frac{1}{\rho} e^{2\alpha} \sqrt{1-e^{-2\alpha}}. \quad (\text{C6})$$

The free energy $\phi_{\alpha,\rho=1}(\lambda)$ is plotted in Fig. 4.

REM free-energy for Spherical patterns

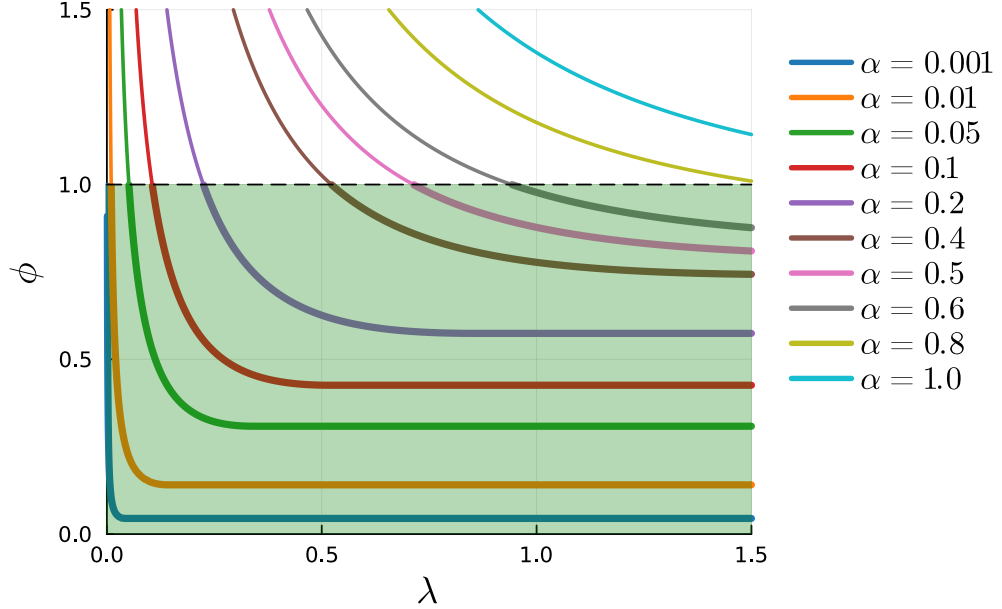


FIG. 4. The REM free energy from Eq. (C5) for the case of spherical patterns as a function of the interaction strength λ and for different loads α . When a curve falls in green region, a typical pattern is retrieved. Also, again in the green region, the value of ϕ correspond to the maxim angle from the pattern $\cos(\theta_c)$ such that the pattern is retrieved, considering random initialization with norm $\rho = \|\mathbf{x}\|/\sqrt{N} = 1$.

The phase boundary for retrieval of a typical pattern, $\alpha_1(\lambda)$ is found by using the expression for $\phi_{\alpha,\rho}$ with $\rho = r = 1$ (which is the radius of any pattern) and finding the value of α such that $\phi_{\alpha,\rho=1}(\lambda) = 1$. This is plotted in Fig. 1 of the Main Text. The retrieval phase boundary is entirely in the region of the REM which is uncondensed.

2. All patterns retrieval

In order to study the retrieval of all patterns using the union bound, we notice that, for the spherical model, all patterns have $r = \|\boldsymbol{\xi}^1\|/\sqrt{N} = 1$. Therefore, Eq. (11) of the Main Text reduces to

$$A(\alpha, \lambda) = \inf_{\phi: \phi > 1} I_{\alpha,1,\lambda}(\phi) \quad (\text{C7})$$

Assuming $\alpha < \alpha_1(\lambda)$, by the very definition of α_1 we have that the typical REM free energy $\phi_{\alpha,r}(\lambda)$ is lower than 1. Therefore, we should look at atypically high free energy. According to Eq. (10) of the Main Text, we have

$$A(\alpha, \lambda) = \inf_{\phi: \phi > 1} \hat{\zeta}_1(\phi) - \alpha. \quad (\text{C8})$$

On the other hand, Eq. (C4) implies that $\hat{\zeta}_1(\phi)$ is finite only for $\phi < 1$. Therefore $A(\alpha, \lambda) = +\infty$ for $\alpha < \alpha_1$ and $A(\alpha, \lambda) = 0$ otherwise. This leads to the final result $\alpha_c^{\text{lb}}(\lambda) = \alpha_c(\lambda) = \alpha_1(\lambda)$ for spherical patterns.

3. Attraction basins

The attraction basins are studied by considering an initial condition \mathbf{x} on the sphere $\|\mathbf{x}\|^2 = N$ sampled uniformly at random but at fixed angle $\cos(\theta) = \mathbf{x} \cdot \boldsymbol{\xi}^1 / N$ from a typical pattern ($\boldsymbol{\xi}^1$ without loss of generality). As argued in the Section of the Main Text discussing basins of attraction, the gradient descent dynamics will converge to $\boldsymbol{\xi}^1$ as long as the initial angle is smaller than some critical angle $\theta_c(\alpha, \lambda)$, that is $\cos(\theta) > \cos(\theta_c)$. The critical angle is found solving $\phi_{\alpha,1}(\lambda) = \cos(\theta_c)$ as suggested by the energy decomposition (3) of the Main Text. The critical lines are shown in Fig. 2 of the Main Text. For a given α , the largest basin size is obtained for $\lambda \geq e^{2\alpha} \sqrt{1 - e^{-2\alpha}}$, where the critical angle becomes $\cos \theta_c = \sqrt{1 - e^{-2\alpha}}$.

For given α and $\rho = \|\mathbf{x}\|/\sqrt{N}$, the basin of attraction for the pattern \mathbf{x}^1 is given by the expression $\rho \cos \theta > \phi_{\alpha,\rho}(\lambda)$ in conjunction with the requirement that $\boldsymbol{\xi}^1$ is a minimum, that is $1 > \phi_{\alpha,1}(\lambda)$. In Fig. 5 we visualize these basins of attraction in the coordinate system $y = \rho \cos(\theta)$, $x = \rho \sin(\theta)$.

Appendix D: Gaussian patterns

1. Typical case

Consider the case where patterns have independent identically distributed components which are Gaussian variables of mean zero and unity variance, and independently choose a vector \mathbf{x} such that $\|\mathbf{x}^2\| = N\rho^2$. Using rotational invariance, the distribution of the energy levels $E^\mu(\mathbf{x}) = \mathbf{x} \cdot \boldsymbol{\xi}^\mu$ depends on \mathbf{x} only through its norm r . One can choose the axes so that $E^\mu(\mathbf{x}) = \rho\sqrt{N}\xi_1^\mu$. The probability density of this energy is expressed by the large deviation function

$$\hat{\zeta}(\varepsilon) = -\frac{1}{N} \log \left[\int \frac{d\xi_1}{\sqrt{2\pi}} e^{-\xi_1^2/2} \delta \left(\varepsilon - \frac{\rho\xi_1}{\sqrt{N}} \right) \right]. \quad (\text{D1})$$

In the large N limit we have

$$\hat{\zeta}_\rho(\varepsilon) = \frac{\varepsilon^2}{2\rho^2} \quad (\text{D2})$$

and

$$\zeta_\rho(\lambda) = \frac{\lambda^2 \rho^2}{2}. \quad (\text{D3})$$

The REM free-energy density, $\phi_{\alpha,\rho}(\lambda)$, is given by

$$\phi_{\alpha,\rho}(\lambda) = \begin{cases} \frac{\alpha}{\lambda} + \frac{1}{2}\lambda\rho^2 & \lambda < \lambda_*(\alpha, \rho) \\ \rho\sqrt{2\alpha} & \lambda \geq \lambda_*(\alpha, \rho), \end{cases} \quad (\text{D4})$$

where

$$\lambda_*(\alpha, \rho) = \frac{\sqrt{2\alpha}}{\rho}. \quad (\text{D5})$$

The free energy $\phi_{\alpha,\rho=1}(\lambda)$ is plotted in Fig. 6.

The phase boundary for retrieval of a typical pattern, $\alpha_1(\lambda)$, is found by using the expression for $\phi_{\alpha,\rho}$ with $\rho = 1$ (which is the radius of a typical pattern) and finding the value of α such that $\phi_{\alpha,1}(\lambda) = 1$. There are two regimes:

- If $0 \leq \lambda < 1$, then $\alpha_1(\lambda) = \lambda(1 - \frac{1}{2}\lambda)$ and the REM is uncondensed.
- If $\lambda \geq 1$, then $\alpha_1(\lambda) = \frac{1}{2}$ and the REM is in its condensed phase.

The resulting phase diagram is plotted in Fig. 3 of the Main Text.

Attraction basins for Spherical patterns

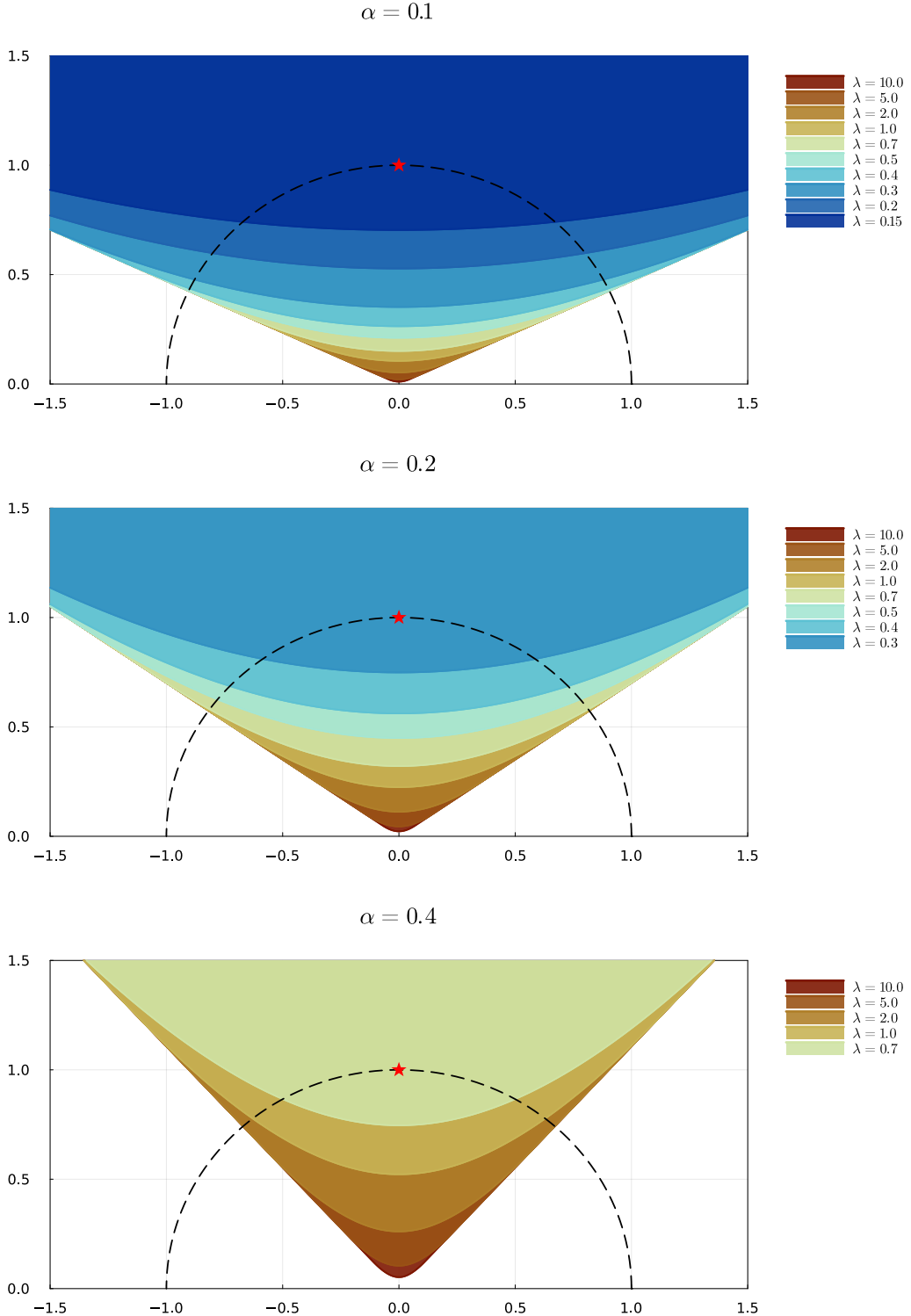


FIG. 5. Basin of attraction (coloured areas) of the pattern ξ_1 (red star), for different values of λ and α . The basins become larger as λ is increased. The dashed line is the unit circle plotted as a visual aid.

REM free-energy for Gaussian patterns

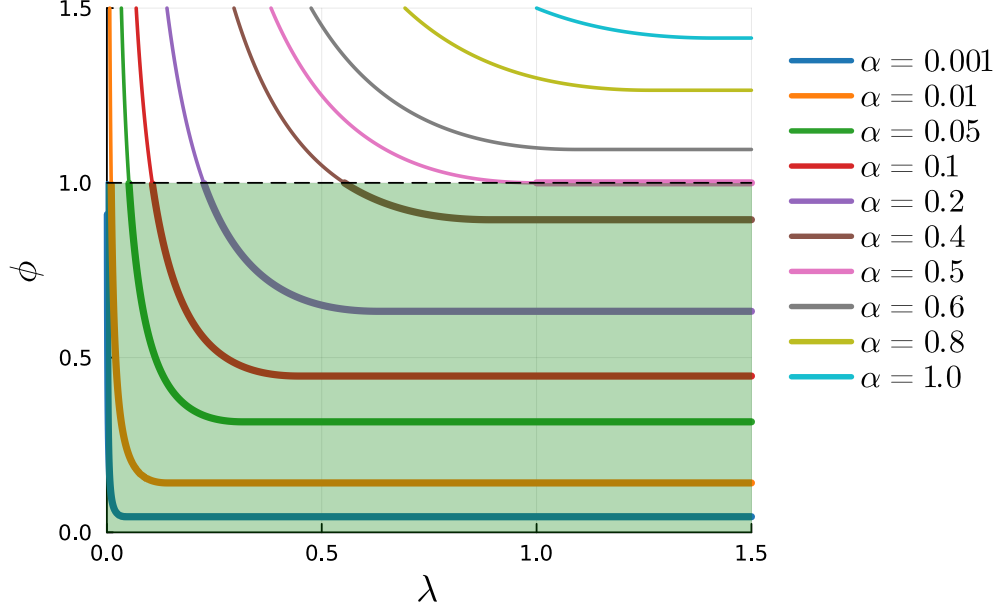


FIG. 6. The REM free energy from Eq. (D4) for the case of Gaussian patterns as a function of the interaction strength λ and for different loads α . When a curve falls in green region, a typical pattern is retrieved. Also, again in the green region, the value of ϕ correspond to the maxim angle from the pattern $\cos(\theta_c)$ such that the pattern is retrieved, considering random initialization with norm $\rho = \|\mathbf{x}\|/\sqrt{N} = 1$.

2. All patterns retrieval

We now compute the quantities involved in the all patterns retrieval lower bound α_c^{lb} given in Eq. (12) of the Main Text. We first compute the large deviation rate function $\tilde{I}(r)$ for the scaled norm of a single pattern, $r = \|\boldsymbol{\xi}\|/\sqrt{N}$. It is easy to show that

$$\tilde{I}(r) = -\lim_{N \rightarrow \infty} \frac{1}{N} \log \int \frac{d^N \boldsymbol{\xi}}{\sqrt{2\pi}^N} e^{-(1/2) \sum_i \xi_i^2} \delta \left(r - \frac{\|\boldsymbol{\xi}\|}{\sqrt{N}} \right) = \frac{1}{2}(r^2 - 1) - \log r. \quad (\text{D6})$$

Then we compute the large deviation function for the REM free energy conditioned on the pattern radius r . According to the general expression in Eq. (10) of the Main Text, this is given by

$$I_{\alpha,r,\lambda}(\phi) = \begin{cases} +\infty & \phi < \phi_{\alpha,r}(\lambda) \\ 0 & \phi = \phi_{\alpha,r}(\lambda) \\ \frac{\phi^2}{2r^2} - \alpha & \phi > \phi_{\alpha,r}(\lambda). \end{cases} \quad (\text{D7})$$

For convenience, we define the function $I^*(\alpha, r, \lambda)$ such that Eq. (11) of the Main Text becomes:

$$A(\alpha, \lambda) = \inf_{r \in [0, \infty)} \tilde{I}(r) + I^*(\alpha, r, \lambda), \quad (\text{D8})$$

that is

$$I^*(\alpha, r, \lambda) = \inf_{\phi: \phi > r^2} I_{\alpha,r,\lambda}(\phi). \quad (\text{D9})$$

Let us denote by $r_0(\alpha, \lambda)$ the value of r such that $r^2 = \phi_{\alpha,r}(\lambda)$. It is given by

$$r_0(\alpha, \lambda) = \begin{cases} \sqrt{\frac{\alpha}{\lambda(1-\lambda/2)}} & 0 \leq \lambda < 1 \\ \sqrt{2\alpha} & \lambda \geq 1. \end{cases} \quad (\text{D10})$$

When $r < r_0$, we have $\phi_{\alpha,r}(\lambda) > r^2$. When $r > r_0$ instead, we have $\phi_{\alpha,r}(\lambda) < r^2$. It follows that:

- If $r > r_0$ the infimum in (D9) is obtained at $\phi = r^2$ and its value is $I_*(\alpha, r, \lambda) = \frac{r^2}{2} - \alpha$.
- If $r < r_0$ the infimum in (D9) is obtained at $\phi = \phi_{\alpha,r}(\lambda)$ and its value is $I_*(\alpha, r, \lambda) = 0$.

This leads to

$$A(\alpha, \lambda) = \min \left(\min_{r \in [0, r_0(\alpha, \lambda)]} \tilde{I}(r), \min_{r \in [r_0(\alpha, \lambda), \infty)} \tilde{I}(r) + \frac{r^2}{2} - \alpha \right). \quad (\text{D11})$$

The final value for $\alpha_c^{\text{lb}}(\lambda)$ is found by solving $A(\alpha, \lambda) = \alpha$. When $\lambda \gtrsim 0.70091$ one gets $\alpha_c^{\text{lb}} = \log(2)/4$. We have $\alpha_c^{\text{lb}} \sim \lambda$ instead for small λ , therefore in this limit it matches $\alpha_1(\lambda)$. The results are shown in Fig. 3 of the Main Text.

3. Attraction basins and typical distances

In the case of Gaussian patterns, the condition $\rho r_\xi \cos(\theta) > \phi_{\alpha,\rho}(\lambda)$ identifying the attraction basin of a typical pattern, for large λ takes the form $\cos(\theta_c) > \sqrt{2\alpha}$. Clearly, the basin disappears when $\alpha > 0.5$.

Since in this ensemble we have large deviations also in the patterns' radii, contrary to the spherical case, we can perform a slightly more refined version of the computation in Appendix B in order to compute also the radius of the patterns with maximum overlap with a reference configuration.

Consider a reference configuration ξ with squared norm $\|\mathbf{x}\|^2 = N$. We ask what is the number of patterns with a certain overlap c with it and with a certain square norm $r^2 N$. That is, we want to compute the statistics of the random variable

$$N(c, r) = \sum_{\mu=2}^P \delta(\mathbf{x} \cdot \xi^\mu - cN) \delta(\|\xi^\mu\|^2 - r^2 N) \quad (\text{D12})$$

Although we are interest in the quenched average, $\frac{1}{N} \mathbb{E} \log N(c, r)$, let's do an annealed computation first.

$$\mathbb{E}N(c, r) = e^{\alpha N} \mathbb{E} \int \frac{d\hat{c}}{2\pi} \frac{d\hat{r}}{2\pi} e^{+i\hat{c}cN + \frac{1}{2}\hat{r}r^2 N - i\hat{q} \sum_i x_i \xi_i - \frac{1}{2}\hat{r} \sum_i (\xi_i)^2} \quad (\text{D13})$$

$$= \int \frac{d\hat{c}}{2\pi/N} \frac{d\hat{r}}{2\pi/N} e^{\alpha N + i\hat{c}cN + \frac{1}{2}\hat{r}r^2 N - \frac{\hat{c}^2}{2(1+\hat{r})} N - \frac{1}{2}N \log(1+\hat{r})} \quad (\text{D14})$$

$$= \int \frac{d\hat{r}}{\sqrt{2\pi(1+\hat{r})/N}} e^{\alpha N + \frac{1}{2}\hat{r}r^2 - \frac{1}{2}c^2(1+\hat{r})N - \frac{1}{2}N \log(1+\hat{r})} \quad (\text{D15})$$

Therefore

$$\lim_{N \rightarrow +\infty} \frac{1}{N} \log \mathbb{E}N(c, r) = \alpha + \frac{1}{2} \text{st}_{\hat{r}} [\hat{r}r^2 - c^2(1+\hat{r}) - \log(1+\hat{r})]. \quad (\text{D16})$$

At the stationary point

$$\hat{r} = \frac{1}{r^2 - c^2} - 1. \quad (\text{D17})$$

This leads to

$$S_\alpha^{ann}(c, r) = \lim_{N \rightarrow +\infty} \frac{1}{N} \log \mathbb{E}N(c, r) = \alpha + \frac{1-r^2}{2} + \frac{1}{2} \log(r^2 - c^2) \quad (\text{D18})$$

A standard second moment argument then gives the concentration of the quenched entropy:

$$S_\alpha(c, r) = \lim_{N \rightarrow \infty} \frac{1}{N} \log N(c) = \begin{cases} S_\alpha^{ann}(c, r) & S_\alpha^{ann}(c, r) \geq 0 \\ -\infty & S_\alpha^{ann}(c, r) < 0 \end{cases} \quad (\text{D19})$$

For a given overlap c , the radius of the patterns giving the dominant contribution to the energy is found by setting $\partial_r S_\alpha^{ann}(c, r) = 0$. This gives

$$r_*(c) = \sqrt{1 + c^2}, \quad (D20)$$

$$S_\alpha^{ann}(c) = S_\alpha^{ann}(c, r_*(c)) = \alpha - \frac{1}{2}c^2 \quad (D21)$$

Imposing the condition $S_\alpha^{ann}(c, r_*(c)) = 0$ we finally recover the result $c_{max} = \sqrt{2\alpha}$.

For given α and $\rho = \|\mathbf{x}\|/\sqrt{N}$, the basin of attraction for the pattern \mathbf{x}^1 is given by the expression $\rho \cos \theta > \phi_{\alpha, \rho}(\lambda)$ in conjunction with the requirement that ξ^1 is a minimum, that is $1 > \phi_{\alpha, 1}(\lambda)$. In Fig. 7 we visualize these basins of attraction in the coordinate system $y = \rho \cos(\theta)$, $x = \rho \sin(\theta)$.

Appendix E: Storage capacity lower bound from Ramsauer et al. '20

In this Appendix, we restate Theorem 3 of Ref. [8] using our notation and we compute its asymptotic form in the high-dimensional limit $N \rightarrow +\infty$ with $P = e^{\alpha N}$ for fixed α . The Theorem considers patterns ξ^μ uniformly distributed on the sphere of radius $K\sqrt{N-1}$ and provides a lower bound for all patterns retrieval capacity at finite N described in the following. We consider $K = 1$ for simplicity and assume failure probability $0 < p \leq 1$ for the storage problem, that is the probability that at least one pattern is not an approximate fixed point of the dynamics (we refer the reader to Ref. [8] for precise definitions). We define the quantities

$$a := \frac{2}{N-1} (1 + \log(2\lambda p(N-1))), \quad b := \frac{2}{5}\lambda, \quad c := \frac{b}{W_0(e^{a+\log b})}; \quad (E1)$$

where W_0 is the upper branch of the Lambert W function. Ensuring $c \geq \left(\frac{2}{\sqrt{P}}\right)^{\frac{N-1}{4}}$, with probability $1-p$ the number of patterns that can be stored P_c satisfies the bound [8]

$$P_c > \sqrt{p} c^{\frac{N-1}{4}}. \quad (E2)$$

We now consider the thermodynamic limit $N, P \rightarrow \infty$ and $p \rightarrow 0$ with:

$$p = e^{-\gamma N}, \quad (E3)$$

$$P_c = e^{\alpha_c N}. \quad (E4)$$

The limit for the previously defined quantities is then

$$a = -2\gamma; \quad b = \frac{2}{5}; \quad \lambda = \frac{2}{5}\lambda \frac{1}{W_0\left(e^{-2\gamma+\log(\frac{2}{5}\lambda)}\right)}. \quad (E5)$$

The inequality (E2) becomes

$$\alpha_c > -\frac{1}{2}\gamma + \frac{1}{4}\log c. \quad (E6)$$

Taking the limit $\gamma \rightarrow 0$ we finally derived the asymptotic form of the bound presented in Ref. [8]:

$$\alpha_c > \frac{1}{4}\log\left[\frac{2\lambda/5}{W_0(2\lambda/5)}\right] =: \alpha_{c, \text{rams}}^{\text{lb}} \quad (E7)$$

For large λ we have $c \sim \frac{2\lambda}{5\log(\frac{2}{5}\lambda)}$ and $\alpha_{c, \text{rams}}^{\text{lb}} \sim \frac{1}{4}\log\lambda$. For small λ instead we have $\alpha_{c, \text{rams}}^{\text{lb}} \sim \lambda/10$. The value of $\alpha_{c, \text{rams}}^{\text{lb}}$ is plotted in Fig. 1 of the Main Text. One can notice a large gap with the exact value obtained by our large deviation analysis.

Attraction basin for Gaussian patterns

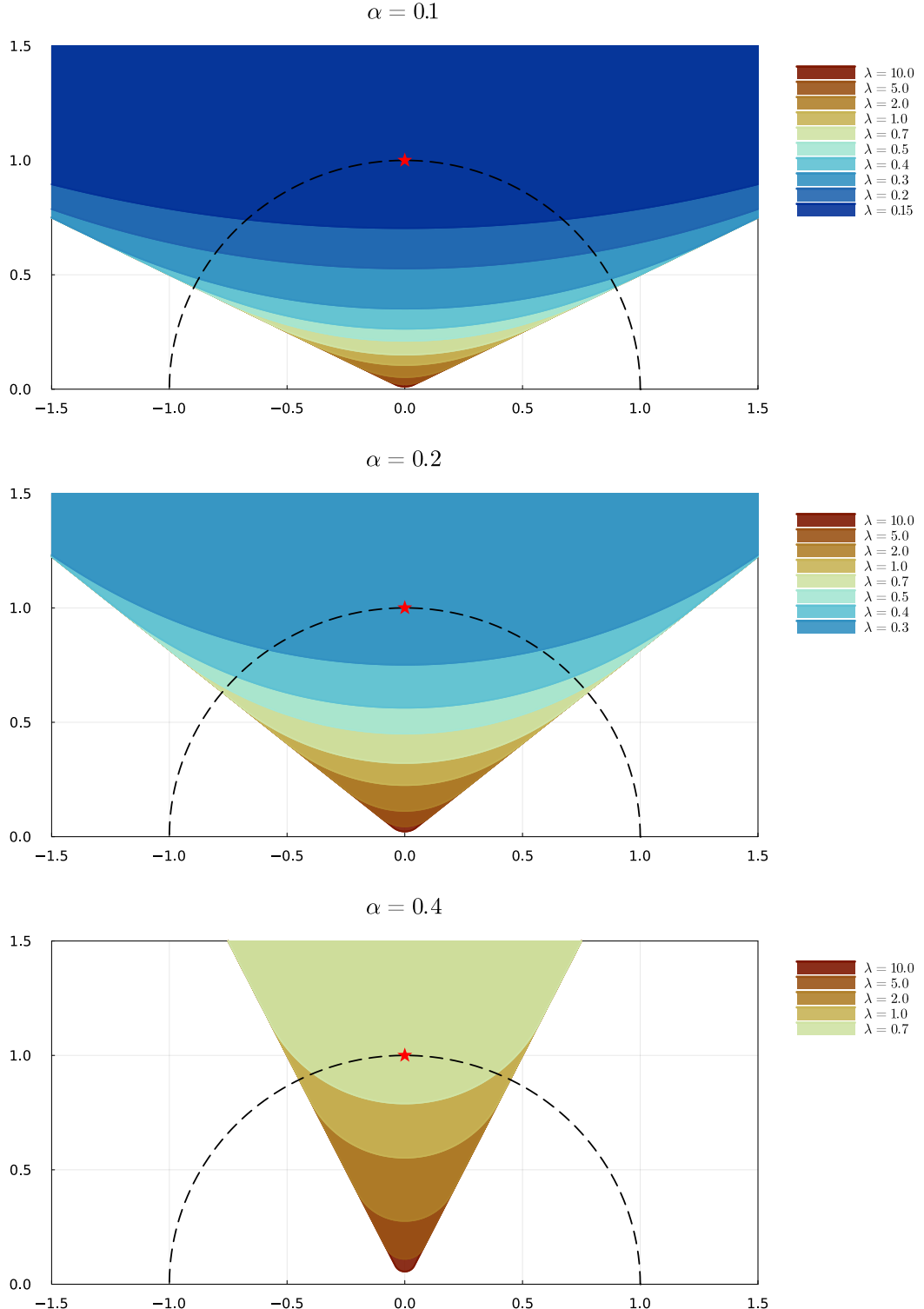


FIG. 7. Basin of attraction (coloured areas) of the pattern ξ_1 (red star), for different values of λ and α . The basins become larger as λ is increased. The dashed line is the unit circle plotted as a visual aid.

Appendix F: Numerical Experiments

This Appendix is devoted to the numerical validation of our analytical result for the typical pattern retrieval threshold $\alpha_1(\lambda)$ (more precisely, we consider its inverse, $\lambda_1(\alpha)$) and for the typical basin size. We make the general remark that while the numerical results are in good agreement with theory predictions for infinite N , dealing with an exponential number of patterns makes the system hard to simulate. We quickly saturate our memory and compute resources going up in N so that is hard to extrapolate the large N behavior. Therefore, the numerical validation of our theory cannot be made entirely satisfactory, and we hope that follow-up works will be able to establish with mathematical rigor our results obtained through partially non-rigorous arguments.

In the numerical experiments, we perform a gradient descent (GD) procedure on the energy function of Eq. (1) of the Main Text. We use a step size $\eta = 0.5$. The results are averaged over a number of realizations of the patterns that vary from 1000 (low values of N and α) to 10 (large N and α).

1. Typical pattern retrieval

In the first set of experiments, we start from the initial condition $\mathbf{x}^{t=0} = \xi^1$ and run GD until convergence. We then plot the normalized distance from the initial configuration, $\Delta = \|\mathbf{x}^{t=\infty} - \xi^1\|^2/N$, as a function of λ and for different values of N and α . The results are presented in Fig. 8 for the spherical case and in Fig. 9 for the Gaussian case. In both cases, at large λ GD remains close to the initial point, meaning that the pattern is an (approximate) minimum. For low λ GD approaches the origin instead, a phenomenon already outlined in Ref. [8] as the "average of all patterns" global fixed point. As expected, the crossover between the two regimes becomes sharper as N increases and approaches the analytical prediction for the threshold $\lambda_1(\alpha)$ obtained by inverting Eq. (9) of the Main Text. We notice that the transition is much smoother in the Gaussian case compared to the spherical case.

In Fig. 10, we present a large N extrapolation in the case of spherical patterns. At given α and N , we define the crossover value of λ as the smallest value of λ for which $\Delta < 0.5$. We then extrapolate the numerical results to large N through a quadratic fit in $\frac{1}{N}$ and compare them with the analytical prediction $\lambda_1(\alpha)$.

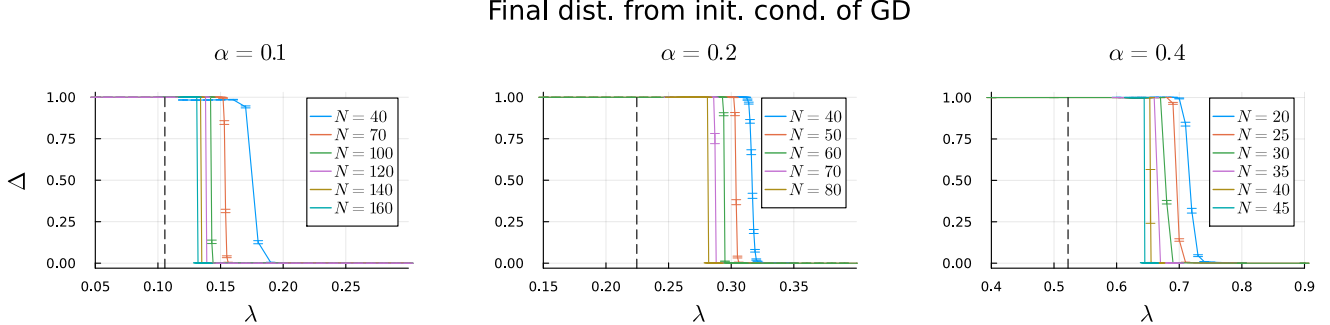


FIG. 8. Spherical patterns. End distance Δ from initial conditions ξ^1 under GD dynamics as a function of the interaction strength λ and for different values of N and α . Vertical lines are the predicted values for the threshold $\lambda_1(\alpha)$ at infinite N separating the retrieval and the non-retrieval regime.

2. Basins

In order to confirm our prediction $\cos \theta_c = \phi_{\alpha,1}(\lambda)$ for the basin size in the case of spherical patterns, we run the following experiments.

We sample an initial configuration for the GD dynamics uniformly at random on the hypersphere of radius \sqrt{N} conditional on it being at a given angle θ from ξ . We then measure the normalized distance of the final configuration from ξ^1 after convergence of GD. The result is shown in Fig. 11 (Left) for $\alpha = 0.1, \lambda = 0.2$ and different values of N as function of $\cos(\theta)$. For small angle ($\cos(\theta)$ close to 1), the final distance is close to 0, therefore the initial configuration lies in the basin of attraction of ξ^1 . Increasing the angle we have a crossover to a regime where the configuration escapes from ξ^1 . As N increases the crossover becomes sharper and approaches the analytical prediction.

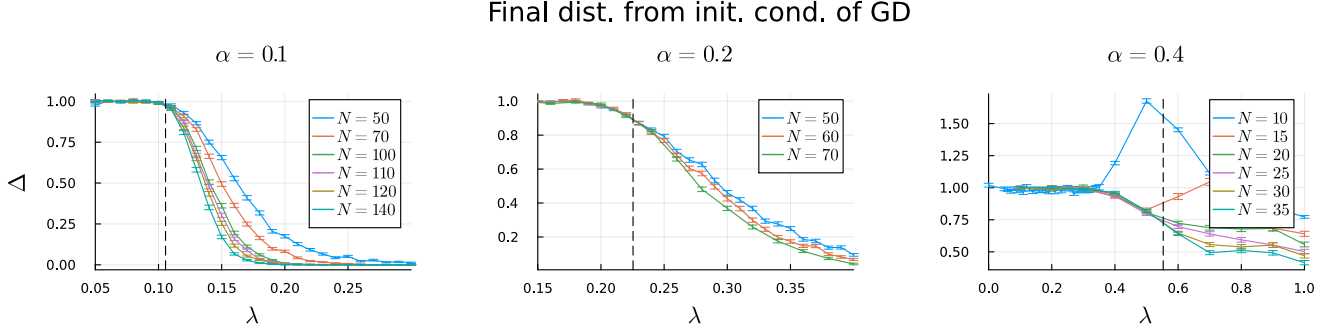


FIG. 9. Gaussian patterns. End distance Δ from initial conditions ξ^1 under GD dynamics as a function of the interaction strength λ and for different values of N and α . Vertical lines are the predicted values for the threshold $\lambda_1(\alpha)$ at infinite N separating the retrieval and the non-retrieval regime.

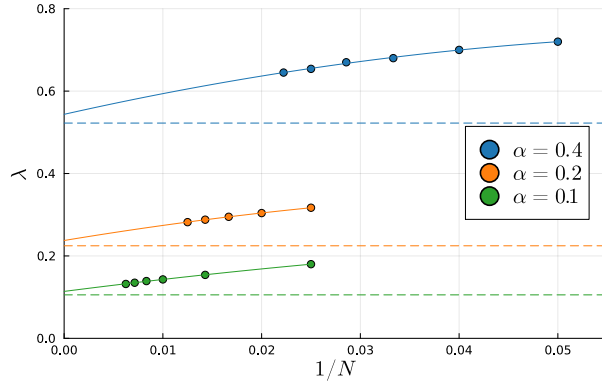


FIG. 10. Gradient descent simulations starting from initial condition ξ^1 . Points correspond to values of λ for which, at fixed α and N , we observe a crossover between a retrieval (higher λ) and non-retrieval (lower λ) phase in the simulations. Solid lines are quadratic fits in $1/N$. Horizontal lines are the predictions from our $N = +\infty$ theory.

In Fig. 11 (Right) we plot the critical angle at finite size N as a function of interaction strength. Since for finite N we don't have sharp thresholds, we define the critical angle as follows: for a given sample, the critical angle is defined as the one for which half of the random initializations of the dynamics (we use 10 restarts) fall back to ξ^1 while the other half escape the basin. We apply a bisection method to find such angle and then average the (cosine of the) angle over 10 samples. As the plot shows, increasing the system size the curves converge to the infinite size theoretical prediction.

3. Scaled dot-product

In Fig. 12 we present numerical validation for the single pattern retrieval threshold $\tilde{\lambda}_1(\tilde{\alpha})$ in the scaling regime where the number of patterns is $P = \exp(\tilde{\alpha}N^{1-\alpha})$ and the energy reads

$$E(\mathbf{x}) = -\frac{N^\alpha}{\tilde{\lambda}} \log \sum_{\mu} e^{\frac{\tilde{\lambda}}{N^\alpha} \mathbf{x} \cdot \xi^{\mu}} + \frac{1}{2} \|\mathbf{x}\|^2. \quad (\text{F1})$$

The numerical protocol is the Gradient Descent one discussed in Appendix F 1. We observe that by increasing N the retrieval crossover approaches the theoretical prediction as expected.

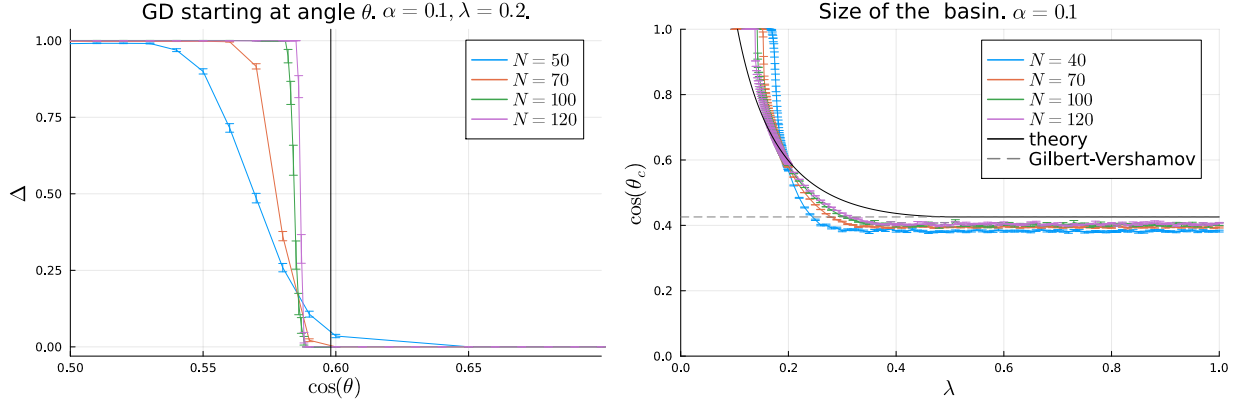


FIG. 11. (Left) Distance Δ from the reference pattern ξ^1 as a function of the starting angle at the end of GD dynamics. We set $\alpha = 0.1$ and $\lambda = 0.2$, with spherical patterns, and simulate different system sizes N . The theory prediction for the critical angle is given by the vertical line. (Right) Critical angle for the basin as a function of interaction strength. Numerical simulations at finite size are compared to the theory prediction for infinite size and to the Gilbert-Vershawov result for the angle of the nearest pattern.

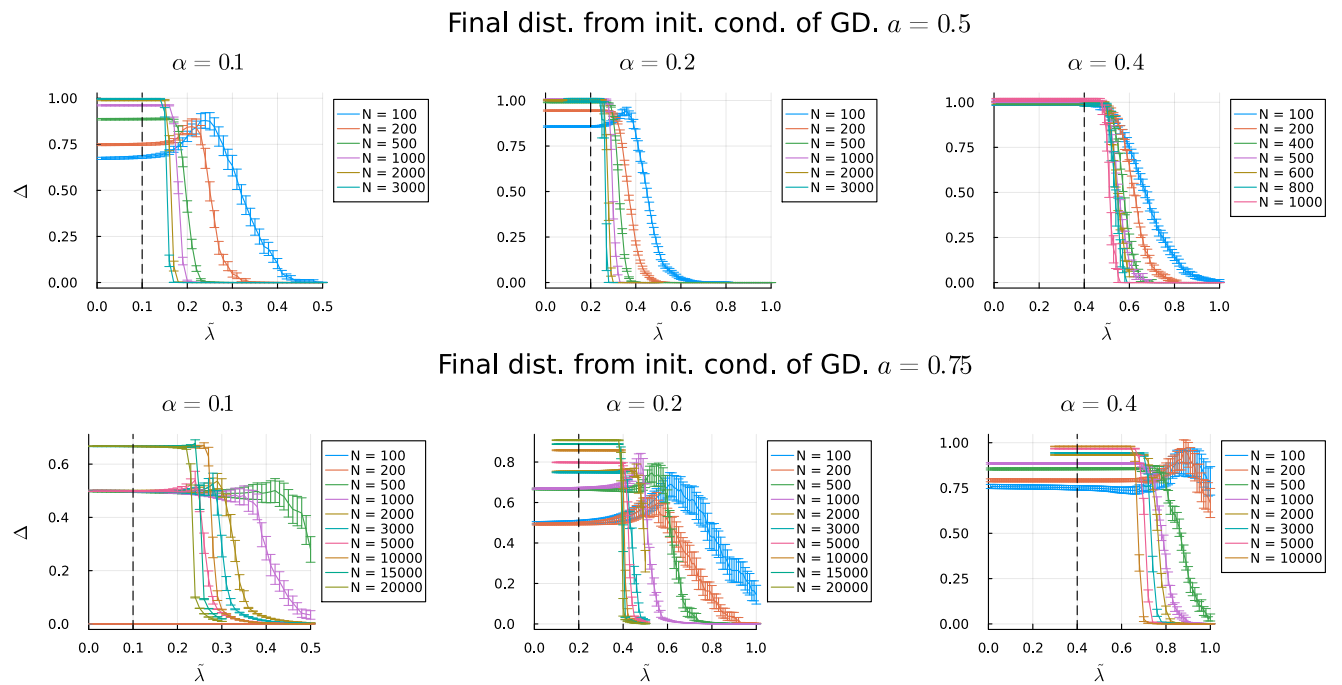


FIG. 12. Final distance from pattern \mathbf{x}^1 after GD iteration for scaled attention with exponents $a = 1/2$ (top) and $a = 3/4$ (bottom). Vertical lines are the theoretical predictions $\lambda_1(\tilde{\alpha}) = \tilde{\alpha}$ for the retrieval transition. The patterns are sampled from the Gaussian ensemble.